**Article:**
Piazolo, S, Belousova, E, Fontaine, AL et al. (2017) Trace element homogeneity from micron- to atomic scale: Implication for the suitability of the zircon GJ-1 as a trace element reference material. Chemical Geology, 456. pp. 10-18. ISSN: 0009-2541

https://doi.org/10.1016/j.chemgeo.2017.03.001

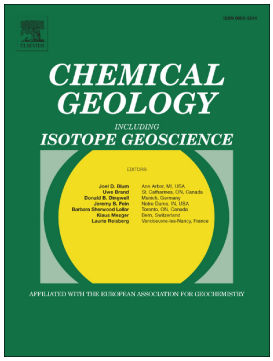


# Trace element homogeneity from micron- to atomic scale: Implication for the suitability of the zircon GJ-1 as a trace element reference material

Sandra Piazolo, Elena Belousova, Alexander La Fontaine, Christopher Corcoran, Julie M. Cairney

PII: S0009-2541(17)30116-X
DOI: doi: 10.1016/j.chemgeo.2017.03.001
Reference: CHEMGE 18269

To appear in: *Chemical Geology*

Received date: 31 August 2016
Revised date: 26 February 2017
Accepted date: 1 March 2017

Please cite this article as: Sandra Piazolo, Elena Belousova, Alexander La Fontaine, Christopher Corcoran, Julie M. Cairney , Trace element homogeneity from micron- to atomic scale: Implication for the suitability of the zircon GJ-1 as a trace element reference material. The address for the corresponding author was captured as affiliation for all authors. Please check if appropriate. Chemge(2017), doi: 10.1016/j.chemgeo.2017.03.001

# Trace element homogeneity from micron - to atomic scale: implication for the suitability of the zircon GJ-1 as a trace element reference material

Sandra Piazolo[1,2,*], Elena Belousova[1], Alexander La Fontaine[3], Christopher Corcoran[1], Julie M. Cairney[3]

[1] Australian Research Council Centre of Excellence for Core to Crust Fluid Systems/GEMOC, Department of Earth and Planetary Sciences, Macquarie University, New South Wales 2109, Australia

[2] School of Earth and Environment, University of Leeds, UK

[3] Australian Centre for Microscopy and Microanalysis, University of Sydney, Sydney, New South Wales 2006, Australia

*Correspondence and requests for materials should be addressed to Sandra Piazolo

(email: s.piazolo@leeds.ac.uk)



## Highlights

- The zircon reference material GJ-1 shows micron- to atomic scale chemical and structural homogeneity
- GJ-1 can be used as a reference material for U-Th-Pb dating and Lu-Hf isotopic studies, but also for trace element analysis
- GJ-1 combines structural and chemical homogeneity with chemical abundance and large sample size and volume
- Atom probe tomography allows assessment of atomic scale chemical homogeneity of minerals e.g. reference materials

## Keywords

zircon, reference material, trace elements, atom probe tomography, nanometre scale, GJ-1

**Abstract**

The quality of a chemical reference material relies on the fact that the composition of the material is homogeneous across all scales. A series of different techniques have been used to evaluate the trace element homogeneity of the GJ-1 reference zircon from the micron - to atomic scale. Cathodoluminescene imaging was conducted along with quantitative crystallographic orientation analysis and trace element analysis using laser ablation inductively coupled plasma mass spectrometry (LA-ICPMS). The nanometre-scale homogeneity was evaluated by analysing five mineral tips using atom probe tomography, which provides atomic scale three dimensional chemical reconstructions with unprecedented spatial resolution. Results show that the GJ-1 reference zircon is homogeneous at all scales, both structurally and chemically. Crystallographic orientation data confirms that this gem quality zircon has no detectable internal crystallographic orientation changes such as crystal-plastic deformation features or cracks. No mineral inclusions were found. Atom probe tomography shows that there is a lack of any chemical clustering or other modes of spatially defined elemental accumulation or depletion for the most abundant trace elements such as Y, Yb and Hf. This finding is supported by LA-ICPMS data revealing homogeneity within the analytical precision. Trace elements of significant abundance include P, Yb, Y, U and Hf, with contents of 30±6, 65±2, 238±5, 284±14 and 6681±57ppm, respectively. Hence, the GJ-1 zircon used as a reference zircon for U-Pb and Hf- isotopic studies is also a suitable zircon reference material for trace element analyses.

## 1. Introduction

The accuracy of trace element (including rare earth element) data in zircon is of increasing importance in geoscience as zircon ($ZrSiO_4$) is now commonly used, not only as a reliable geochronometer utilizing the U-Th-Pb isotope systems, but also as a trace element monitor. The tendency of the accessory mineral zircon to incorporate trace elements (including radionuclides) and its robustness against both chemical and physical alteration after growth as well as extremely sluggish diffusive re-equilibration at high temperatures contribute to the high fidelity of the zircon trace element record (e.g. Cherniak et al., 1997a; Cherniak et al.,

1997b; Watson and Cherniak, 1997; Cherniak and Watson, 2003; Hoskin and Schaltegger 2003). Many trace elements tend to participate in a coupled substitution within the zircon crystal structure and therefore behave relatively coherently. Phosphorus concentrations, for example, correlate positively with Y and REEs (rare earth elements), reflecting the so-called xenotime substitution $(REE, Y)^{3+} + P^{5+} = Zr^{4+} + Si^{4+}$ (Belousova et al., 2002). Many other coupled substitutions may occur within zircon (e.g. Reid et al., 2011), although it has also been shown that elements such as Li and Al tend to occur interstitially (Bouvier et al., 2012).

In recent years, the usefulness of zircon trace element data has been rigorously tested and developed into a tool used in igneous source rock determination (Belousova et al., 2002; Grimes et al., 2007; Grimes et al., 2015; Chapman et al., 2016) as well as petrogenetic modelling (Belousova et al., 2006). In addition, trace element ratios become increasingly important. For example, zircon incorporates ~1 wt.% of Hf into its crystal structure (e.g. Patchett et al., 1981; Claiborne et al., 2006). As Hf is nearly exclusively incorporated into zircon, it controls the Hf budget of most crustal rocks (Wark & Miller, 1993). At the same time, Lu occurs in relatively low concentrations in the range of a few tens of ppm; hence zircons usually have a low Lu/Hf ratio. Because of this very low Lu/Hf ratio, zircon can preserve the $^{176}Hf/^{177}Hf$ of its parental magma at the time of crystallization and, when combined with U-Pb analysis, this mineral has provided unprecedented insight into crustal evolution (e.g. Vervoort and Blichert-Toft, 1999; Amelin et al., 2000; Griffin et al., 2000; Kemp et al., 2005; Belousova et al., 2006; Scherer et al., 2007; Belousova et al., 2010) and sedimentary provenance (e.g. Andersen, 2005; Griffin et al., 2006). Routine zircon analyses of U-Pb, Hf-isotope and other trace elements using LA-ICPMS and LA-MC-ICPMS have increased dramatically in recent years (Blichert-Toft et al., 1997; Belousova et al., 2010).

The increase in this type of analysis has created a need within the geological community of well-characterized reference materials to monitor instrumental drift and to define external reproducibility. Such a reference material is a material that is "sufficiently homogeneous and stable with reference to specified properties, which has been established to be fit for its intended use in measurement or in examination of nominal properties" (Potts, 2012). While geochemical analysis is becoming increasingly common mainly using in-situ LA_ICPMS analysis, this type of analysis is highly destructive. Consequently, there is an ever increasing demand for chemically homogeneous, well-characterized reference material for zircons. Over the decade, the GJ-1 reference zircon developed at GEMOC/CCFS (Macquarie

University, Sydney, Australia) has been widely distributed as a reference zircon for U-Pb geochronology and Hf-isotope analyses (e.g. Jackson et al., 2004; Elhlou, et al., 2006; Morel et al., 2008; Nasdala et al., 2008; Frei & Gerdes, 2009; Matteini et al., 2010; Cottle et al., 2012; Košler et al., 2013).

At the same time, over the last decade it has been shown that elements within zircon can be heterogeneously distributed at the micrometre scale (e.g. Reddy et al., 2006, 2007, 2009; Timms et al., 2006; Piazolo et al., 2012; Hofmann et al., 2009, 2014). In addition, recent studies using now commonly available advanced techniques such as scanning ion imaging have revealed that zircons previously thought to be homogeneous in isotopic and trace elemental composition can exhibit significant elemental clustering at the submicron scale (e.g. Kusiak et al., 2013a, 2013b; Kovaleva et al., 2015).

Recent advances in atom probe tomography (APT) now allow analysis of non-conductive minerals such as zircon in terms of trace element homogeneity or heterogeneity at the nanometre scale. More specifically, ATP provides three-dimensional visualization and chemical identification of materials at the atomic scale (Gault et al., 2012). In this technique, ions are successively field-ionised from the tip of a needle shaped sample (approximately 160-240nm width, 800-1200nm length), collected by a position sensitive detector and their mass-to-charge ratios recorded by time-of-flight spectrometry. From this data, a three dimensional reconstruction of the field-evaporated volume is obtained consisting typically of millions of atoms. Due to the successive field evaporation of atoms from the end of the atom probe tip, the sample tip is destroyed during the analysis. Valley et al. (2014) utilized APT to investigate zircon from the oldest known zircon suite (Jack Hills zircons). They found that trace elements such as Y and Pb could cluster at the nanometre scale due to inferred prolonged heating. Recently, APT has been used to observe deformation-induced redistribution of trace elements within zircon grains from the Archean Napier Complex, Antarctica (Piazolo, et al., 2016). In their study, Piazolo et al. (2016) successfully explain the origin of reverse and normal discordance commonly observed in zircons and their link to structural variations induced by crystal-plastic deformation. They found that dislocations that move through the crystal lattice of zircons tend to accumulate Al, Y, and U, while pipe diffusion along dislocation arrays can lead to preferential removal of certain elements (e.g. Pb) resulting in enriched chemical or structural sinks towards the end of dislocation arrays. As a result of this process, trace elements are redistributed and thus their spatial distribution is heterogeneous at the atomic to micrometre scale.

Here, we analyse in detail the GEMOC GJ-1 zircon reference material (crystal #81) in order to assess its chemical and structural homogeneity from the micron to the atomic scale. GJ-1 zircons have been used since 2002 (e.g. Spetsius et al., 2002), primarily as a zircon reference material for U-Pb dating (e.g. Jackson et al., 2004; Gerdes & Zeh, 2006; Zheng et al., 2006), but also for Hf-isotope analysis (e.g Elhlou et al., 2006; Gerdes & Zeh, 2006; Griffin et al., 2006; Yuan et al., 2008; Matteini et al., 2010). Individual grains are commonly between 0.7 and 1 cm in size and are thought to originate from African pegmatites with a crystallization age of 608.5±0.4 Ma (Jackson et al., 2004; Elhlou et al. 2006).

We show that the GJ-1 zircon reference material is exceptionally homogeneous even at the atomic scale and is therefore not only a reliable reference material for U-Pb dating and Hf-isotope studies but also for trace and rare earth element analysis. Therefore, we envisage that users will utilize GJ-1 not only as a reference material for U-Pb and Hf isotope analysis but also for trace element analysis; an analysis more and more frequently used. In addition, our study demonstrates that APT which provides three-dimensional atomic scale elemental reconstructions is an appropriate technique to assess the suitability of analytical reference materials at the nanometre scale.

## 2. Methods

### *2.1. Cathodoluminescence (CL) imaging and quantitative crystallographic orientation analysis*

To evaluate the homogeneity of the zircon, CL imaging was performed on a Zeiss EVO SEM with a tungsten source operated at 15 kV under high vacuum.

We conducted two sets of quantitative crystallographic orientation analyses, namely electron backscatter diffraction (EBSD) and transmission Kikuchi diffraction (TKD), to test if there was any distortion of the crystallographic lattice at the micron and nanometre scale, respectively. ESBD analysis was conducted on the polished reference zircon embedded in epoxy, while TKD analysis was conducted on the ATP tip before ATP analysis (for details of the preparation of the atom probe tip see below). To prepare for EBSD analysis a colloidal silica–water solution (mixed in proportion 80:20) was used at the final stage of polishing for 3 – 5 minutes to reduce surface damage produced by mechanical polishing. Subsequently the sample was carbon-coated. We used the HKL NordlysNano high sensitivity Electron

Backscatter Diffraction (EBSD) detector and indexed with AzTec analysis software (Oxford Instruments) at the Geochemical Analysis Unit (GAU, Macquarie University). The analysis was carried out on the sample tilted to 70° angle, in high vacuum conditions with 20 kV accelerating voltage, at a beam current of 8.2 nA and at working distances of 12 mm. The EBSD map was acquired by point analysis on a regular grid with a step size of 8 µm. Transmission Kikuchi diffraction (TKD) provides orientation information with a higher spatial resolution than EBSD (Trimby, 2012; Trimby et al., 2014) allowing characterisation of plastic deformation within the tip and subsequent correlation with atom probe data. The TKD signal arises from the lower surface of the tip, so that a boundary of any misorientation would only be apparent where it intersects the lower surface and at the very tip end. TKD was performed using step sizes of 10 and 20 nm and acceleration voltages of 15 and 30 kV, respectively.

For both datasets we used the post-acquisition processing software suite Channel 5 from HKL Technology (Oxford Instruments). The resulting EBSD map contained a maximum of 8% non-indexed points (zero solutions), mostly resulting from polishing-induced scratches, especially for the overview map of the GJ-1/81 grain. The map quality was improved by a "standard" noise reduction following the procedures of Prior et al. (2002) and Piazolo et al. (2006).

*2.2. Laser Ablation Inductively Coupled Plasma Mass Spectrometry (LA-ICPMS)*

LA-ICPMS trace element concentrations were measured in-situ using a Photon Machines Analyte Excite Excimer Laser Ablation System (193 nm) attached to an Agilent 7700cx quadrupole ICPMS. The laser parameters were chosen to ensure maximum accuracy and sensitivity for trace element analysis including light rare earth elements. Parameters were as follows: 5 Hz frequency, 65 µm spot size, fluence of 7.59 J/cm$^2$ and energy set point of 4.5 mJ. This resulted in a laser pit depth of approximately 40 µm. Quantitative results for the trace elements reported here were obtained through calibration of relative element sensitivities using the NIST-610 standard glass as the external calibration standard and Zr content was used for internal calibration. Two NIST-610 standards were analysed before and after each analysis series, which consisted of 10 GJ-1 zircon analyses. The analysis of a basaltic reference standard BCR-2 was run before the unknowns as an independent control on reproducibility and instrument stability (Table 1), with the results well within the recommended and information values of the US Geological Survey

(https://crustal.usgs.gov/geochemical_reference_standards/basaltbcr2.html#information). This set-up of calibration against both NIST-610 and BCR-2 ensured well defined precision and accuracy of data presented. Two series of ten GJ-1 analyses were done, resulting in twenty analyses arranged linearly across the whole sample (Fig. 1). The spots were sufficiently spaced and organized to capture a reasonable spread of values if there were any chemical heterogeneities within the sample (cf. Fig. 1b).

The data acquired included the common trace elements in zircon (Table 2). In addition, to monitor if any inclusion such as allanite, apatite, monazite, and Fe-Ti-Ni oxides were hit, Fe, Mg, Ti, Ni and Ca data was also collected. The data collected were reduced using GLITTER (GEMOC Laser ICPMS Total Trace Element Reduction) software – an online interactive software that was used during the analyses to inspect and evaluate the data in real time and to observe the quantitative trace element analyses with dynamically linked graphics and analysis tables (www.mq.edu.au/GEMOC; Griffin et al., 2008).

### *2.3. Atom Probe Tomography: Sample preparation, data acquisition details, elemental reconstruction procedure and data analysis methods*

Sample preparation, data acquisition and analysis for ATP analysis was conducted at the Australian Centre for Microscopy and Microanalysis (ACMM) at the University of Sydney. Sites for tip removal were selected avoided previous ablated areas. After the sample was removed from its epoxy puck using a diamond saw, it was cut into small pieces and was then prepared using the wedge method (Gault et al., 2012; Saxey et al. 2007). First the samples were pre-thinned using a tripod system to manually polish the grains on increasingly finer diamond coated sheets. Once sufficiently thin wedges were acquired, they were attached to small slotted grids for support. The wedges were cut into atom probe tips using a Zeiss Auriga focussed ion beam scanning electron microscope (FIB-SEM). A $Ga^+$ ion beam was used to cut away material from the sides of the sample and annular milling was used to shape the tips from the edge of the samples to obtain a desirable diameter (80-120 nm) keeping them as smooth as possible. Lower final acceleration voltages were used in order to avoid Ga implantation within the grains as well as any possible damage.

The atom probe tips were analysed using a CAMECA LEAP 4000 X Si atom probe, which is equipped with a picosecond-pulse ultraviolet laser. In our study, the APT analysis chamber and the sample were cooled to cryogenic temperatures (~ 50 K) and maintained at ultra-high vacuum (~ $10^{-11}$ torr). For analysis, a 355 nm-wavelength laser with a pulse energy of 400 pJ

and 250 kHz pulse frequency was used to field evaporate the samples at 50 K. A total of ~ 70 million atoms from 5 tips were detected, where datasets from individual atom probe tips varied between 7 and 22 million atoms.

## 3. Results and Discussion

### *3.1. General sample characteristics – mm to micron scale overall chemical and structural homogeneity*

The zircon analysed is gem quality with no optically visible flaws such as cracks, discolouration or chemical zonation (Fig. 1a). CL imaging reveals no visible banding, zonation or inclusions and proves the overall homogeneity of the reference material in terms of CL-active elements, which is consistent with the results obtained for GJ-1 reference materials previously by Morel et al. (2008) and Jackson et al. (2004) (Fig. 1b). EBSD analysis supports the structural homogeneity of the zircon as suggested by its optical and CL properties as no distinct areas of different crystallographic orientation are seen within the crystal (Fig. 2). It should be noted that slight variations in orientation are due to artefacts such as polishing scratches and surface irregularities.

### *3.2. Laser ablation ICPMS analysis – mm to micron scale chemical homogeneity of trace and rare earth elements*

Data from the laser ablation analysis shows that the GJ-1/81 reference zircon is extremely homogeneous at the scale of the whole crystal (Fig. 3). A traverse across the crystal shows that the variations are within the analytical accuracy of the technique (Table 2, Fig. 3). In general, the GJ-1 zircon is characterised by a relatively low and flat rare earth element (REE) chondrite normalised pattern with a strongly pronounced Ce anomaly and almost complete absence of Eu anomaly (Fig. 3). GJ-1/81 zircon has trace element composition typical of continental-crust zircons according to the U/Yb versus Y discriminant diagram proposed by Grimes et al. (2007, Fig. 4). Trace elements in the GJ-1 zircon are comparable to zircons from low-$SiO_2$ alkaline rocks such as lamproites and carbonatites (Fig. 5). This affinity is supported by the relatively low U and Th content (234±14 ppm and 9.8±0.3 ppm, respectively, Table 2). In Hf (wt%) versus Y (ppm) space (Fig. 6) the GJ-1 reference material falls on the border between alkaline magmatic rocks and carbonatites.

Though the host rock of GJ-1 zircons is not known, the physical and chemical characteristics of these zircons allow us to constrain their origin. The large size of crystals suggests rapid growth from a Zr-rich source with rapid elemental transport in a highly homogenised and stable fluid-rich environments. Pegmatite veins or hydrous highly, evolved melts are possible candidates (e.g. Elhlou et al., 2006). However, such megacrystic zircons have so far only reported from subaluminous/metaluminous pegmatites (Černý & Ercit 2005). The large grain size and chemical homogeneity observed in CL, both relatively unusual characteristics for zircon, have been interpreted as signatures for a metasomatic/vein-related origin as these environments are characterized by the necessary fast elemental transport and open chemical system (e.g., Rubatto, 2002; Hoskin and Schaltegger, 2003; Hoskin, 2005). Interestingly, a lack of an Eu anomaly is a common signature of zircons from alkaline melts which suggests crystallization in absence or before plagioclase crystallization (e.g. Belousova et al., 2002), precluding an origin from a high Si melt/fluid. The Eu anomaly is consistent with the frequently observed near-lack of Eu anomaly in carbonatites (e.g. Belousova et al., 2002), even tough there are some reports of an Eu amomaly between 0.3 and 0.7 carbonatite zircons (Schmitt et al., 2010). The remarkable amplitude of Ce anomaly observed for the GJ zircon is similar to that reported previously for zircons from syenite and nepheline syenite pegmatites (e.g. Belousova et al., 2002; Fig. 6d) and most likely reflects a highly oxidizing conditions during crystallization. In summary, the homogeneity in chemistry, trace element content and size of the zircons suggest that the GJ-1 zircon likely originated from a metasomatic to pegmatitic vein of low Si, carbonatitic to subalumineous composition.

### *3.3. Atom probe tomography data – nanometre-scale chemical homogeneity of major, trace and rare earth elements*

Data from the five tips analysed consistently show that, at the nanometre-scale, the GJ-1/81 reference zircon is chemically homogeneous for all the elements detected (Fig. 7a). We do not observe any elemental clustering, as previously observed for another zircon (Valley et al., 2014, 2015; Piazolo et al., 2016) (Fig. 7c). This chemical homogeneity is coupled with structural homogeneity, where the variation in crystallographic orientation is within range of the analytical error range of the technique (0.3°; Fig. 7b). To illustrate that the apparent chemical homogeneity is not an artefact of the technique itself, we compare a similar dataset (DN77) to that of the GJ-1 reference material. Both datasets have similar bulk levels of Y (100-200 ppm), however the dataset DN77 exhibits significant elemental clustering of Y at the nanometre scale which is clearly visible in the 3D representation of the atom probe tip

(Fig. 7c). This clustering is spatially associated with distinct changes in crystallographic orientation i.e. low angle boundaries which are interpreted to originate from crystal plastic deformation at high temperature (Fig. 7d). In the case of dataset DN77, the observed clustering is associated with dislocation related elemental redistribution similar to those described and interpreted by Piazolo et al. (2016). Both the clustering and the presence of orientation changes are in contrast to the lack of such features in the case of the GJ-1/81 zircon (Fig. 7).

Due to technical constraints it is not possible to detect with confidence all trace and rare rare-earth elements detectable by LA-ICPMS. This limitation stems largely from the fact that ATP uses time of flight mass spectroscopy to identify the elements, hence the relative peak positions of different elements is crucial as peak overlaps prevent quantification of some elements with satisfactory confidence. Furthermore, sufficiently high numbers of atoms are required to be detected to allow unequivocal identification of the presence of the respective element (for details see Valley et al., 2015; La Fontaine et al., 2017). Nevertheless, since trace and rare earth elements in minerals commonly show similar changes in pattern (e.g. Piazolo et al., 2016) or specific elements are substituted by other elements to retain charge balance, e.g. $(REE, Y)^{3+} + P^{5+} = Zr^{4+} + Si^{4+}$ (Belousova, et al., 2002), the lack of clustering in $Y^{3+}$, $P^{5+}$, $Zr^{4+}$ and $Si^{4+}$ suggests that even those elements that cannot reliably be detected using ATP are not heterogeneously distributed throughout the GJ reference material.

In summary, even though it is only possible to detect elements with concentrations above approximately 20 ppm (depending on peak position in the mass spectrum and number of ions collected), ATP is a powerful technique to evaluate the possible clustering of elements within a crystalline lattice. This allows for evaluation of the suitability of analytical reference materials at a time when the spatial resolution of in-situ analytical methods becomes more and more refined.

*3.4. GJ1 – a suitable trace and rare earth element reference zircon*

Material that can be utilized as a analytical reference material needs to meet a number of criteria: (I) chemical homogeneity allowing high confidence in the reproducibility of data, (II) absence of structural heterogeneities including inclusions as these would result in chemical heterogeneities, (III) sufficiently large grains to allow multiple analyses; this feature is especially important if the analytical technique used is destructive i.e. significant material loss occurs, and (IV) sufficient quantities of grains allowing use of the same reference

material across different laboratories and sample series. In search of a reference zircon suitable for trace and rare earth elements, several categories of zircon can be evaluated including magmatic zircons of variable origin and metamorphic zircon. Typical magmatic zircon of crustal origin ranges in size from about 20 to 200 μm and may occur in high abundance in some felsic rocks. Therefore these could, at least in terms of abundance and size, serve as reference materials. However, magmatic continental crustal zircons are characterized by the presence of well-developed growth zoning originating from crystallization in a changing chemical environment (e.g. Vavra, 1990; Schaltegger et al., 1999; Grimes et al., 2015). This zoning reflects compositional variation of Zr and Si and more importantly, variations in Hf, P, Y, the REE, U and Th, up to an order of magnitude for some of these elements (e.g. Corfu et al., 2003). Metamorphic zircons are also commonly small and exhibit large variations in trace element content even within the same rock type (e.g. Rubatto, 2002; Chen et al., 2010); hence also those are unsuitable to serve as zircon reference materials. In addition, production of potential reference material using laboratory zircon crystallization via flux or hydrothermal synthesis has had only limited success because of the small and/or heterogeneous zircon that resulted from these experiments (Hanchar et al., 2001). In summary, large variation in trace element content within single crystals and/or relatively small grain sizes makes zircons originating from most common igneous and metamorphic rock types unsuitable for chemical reference materials.

In contrast to common magmatic and metamorphic zircons, the relatively large size of the GJ-1 zircon crystals and homogeneous internal structure and composition suggest their crystallization or equilibration under physically and chemically very stable conditions. Hence, gem-quality GJ zircon is unique and one of the few zircon populations that can be used as an analytical reference material.

## 4. Conclusion

Only in highly homogenised and stable fluid-rich environments can compositionally and structurally homogeneous zircons of gem quality be produced to provide a reliable reference material. Our analysis of the zircon GJ-1/81 reference material shows that this zircon is ideally suited as a reference material not only for U-Th-Pb dating (Jackson et al., 2004) and Lu-Hf isotopic studies (Morel et al. 2008), but also for trace element al analysis. The chemical homogeneity of the GJ-1 reference material from micrometre - to mm scale is

confirmed by LA-ICPMS analysis and CL imaging, respectively, while the structural homogeneity is established using EBSD and TKD analysis.

Importantly, for the first time it can be shown that the elemental homogeneity is carried through to the atomic scale by using ATP, which allows three-dimensional chemical reconstructions of nanometre-sized sample volumes at atomic resolution.

**Acknowledgements**

This work is supported by the Australian Research Council through DP120102060 and FT1101100070 to SP, and FT110100685 to EB. The authors acknowledge the facilities, and the scientific and technical assistance, of the Australian Microscopy & Microanalysis Research Facility at the Australian Centre for Microscopy and Microanalysis, University of Sydney. Special thanks to P. Trimby and to L. Yang for assistance with the TKD analysis and initial sample preparation, respectively. Bill Griffin is recognised for obtaining and providing GEMOC/CCFS with GJ zircon material and S. Harley is acknowledged for provision of sample DN77 for comparison. This is contribution XX from the ARC Centre of Excellence for Core to Crust Fluid Systems (http://www.ccfs.mq.edu.au) and XX in the GEMOC Key Centre (http://www.gemoc.mq.edu.au).

**References**

Amelin, Y., Lee, D.-C., Halliday, A.N. 2000. Early-middle Archaean crustal evolution deduced from Lu–Hf and U–Pb isotopic studies of single zircon grains. Geochimica et Cosmochimica Acta 64, 4205–4225.

Andersen, T. 2005. Detrital zircons as tracers of sedimentary provenance: limiting conditions from statistics and numerical simulation. Chemical Geology 2163, 249-270.

Belousova, E. A., Griffin, W. L., & Pearson, N. J. 1998. Trace element composition and cathodoluminescence properties of southern African kimberlitic zircons. Mineralogical Magazine 62, 355-366.

Belousova, E., Griffin, W. L., O'Reilly, S. Y., & Fisher, N. L. 2002. Igneous zircon: trace element composition as an indicator of source rock type. Contributions to Mineralogy and Petrology 143, 602-622.

Belousova, E. A., Griffin, W. L., & O'REILLY, S. Y. 2006. Zircon crystal morphology, trace element signatures and Hf isotope composition as a tool for petrogenetic modelling: examples from Eastern Australian granitoids. Journal of Petrology 472, 329-353.

Belousova, E.A., Kostitsyn, Y.A., Griffin, W.L., Begg, G.C., O'Reilly, S.Y. and Pearson,N.J. 2010. The growth of the continental crust: Constraints from zircon Hf-isotope data. Lithos 119, 457-466.

Blichert-Toft, J., Chauvel, C., & Albarède, F. 1997. Separation of Hf and Lu for high-precision isotope analysis of rock samples by magnetic sector-multiple collector ICP-MS. Contributions to Mineralogy and Petrology 127, 248-260.

Bouvier, A. S., Ushikubo, T., Kita, N. T., Cavosie, A. J., Kozdon, R., & Valley, J. W. 2012. Li isotopes and trace elements as a petrogenetic tracer in zircon: insights from Archean TTGs and sanukitoids. Contributions to Mineralogy and Petrology 163, 745-768.

Černý, P., & Ercit, T. S. 2005. The classification of granitic pegmatites revisited. The Canadian Mineralogist, 43.

Chapman, J. B., Gehrels, G. E., Ducea, M. N., Giesler, N., & Pullen, A. 2016. A new method for estimating parent rock trace element concentrations from zircon. Chemical Geology 43, 59-70.

Cheadle, M. J., & John, B. E. 2015. "Fingerprinting" tectono-magmatic provenance using trace elements in igneous zircon. Contributions to Mineralogy and Petrology 170, 1-26.

Chen, R. X., Zheng, Y. F., & Xie, L. 2010. Metamorphic growth and recrystallization of zircon: distinction by simultaneous in-situ analyses of trace elements, U–Th–Pb and Lu–Hf isotopes in zircons from eclogite-facies rocks in the Sulu orogen. Lithos 114, 132-154.

Cherniak, D. J., Hanchar, J. M., & Watson, E. B. 1997. Rare-earth diffusion in zircon. Chemical Geology 134, 289-301.

Cherniak, D. J., Hanchar, J. M., & Watson, E. B. 1997. Diffusion of tetravalent cations in zircon. Contributions to Mineralogy and Petrology 127, 383-390.

Cherniak, D. J. & Watson, E. B. 2003Diffusion in zircon. Reviews in Mineralogy and Geochemistry 53, 113-143.

Claiborne, L. L., Miller, C. F., Walker, B. A., Wooden, J. L., Mazdab, F. K., & Bea, F. 2006. Tracking magmatic processes through Zr/Hf ratios in rocks and Hf and Ti zoning in zircons: an example from the Spirit Mountain batholith, Nevada. Mineralogical Magazine 70, 517-543.

Corfu, F., Hanchar, J.M., Hoskin, P.W.O., Kinny, P. 2003. Atlas of Zircon Textures. – In: Hanchar, J.M.; Hoskin, W.O. Eds. Zircon: Reviews in Mineralogy and Geochemistry 53, 468 – 500, Washington.

Cottle, J. M., Kylander-Clark, A. R., & Vrijmoed, J. C. 2012. U–Th/Pb geochronology of detrital zircon and monazite by single shot laser ablation inductively coupled plasma mass spectrometry SS-LA-ICPMS. Chemical Geology 332, 136-147.

Elhlou, S., Belousova, E., Griffin, W. L., Pearson, N. J., & O'Reilly, S. Y. 2006. Trace element and isotopic composition of GJ-red zircon material by laser ablation. Geochimica et Cosmochimica Acta, 70, A158.

Fisher, C. M., Hanchar, J. M., Samson, S. D., Dhuime, B., Blichert-Toft, J., Vervoort, J. D., & Lam, R. 2011. Synthetic zircon doped with hafnium and rare earth elements: a reference material for in situ hafnium isotope analysis. Chemical Geology 286, 32-47.

La Fontaine, A., Piazolo, S., Trimby, P., Yang, L. and Cairney, J.M. 2017. Laser-Assisted Atom Probe Tomography of Deformed Minerals: A Zircon Case Study. Microscopy and Microanalysis, 1-10.

Frei, D., & Gerdes, A. 2009. Precise and accurate in situ U–Pb dating of zircon with high sample throughput by automated LA-SF-ICP-MS. Chemical Geology 261, 261-270.

Gault, B., Moody, M. P., Cairney, J. M., & Ringer, S. P. 2012. Atom probe microscopy Vol. 160. Springer Science & Business Media.

Gerdes, A., & Zeh, A. 2006. Combined U–Pb and Hf isotope LA-MC- ICP-MS analyses of detrital zircons: comparison with SHRIMP and new constraints for the provenance and age of

an Armorican metasediment in Central Germany. Earth and Planetary Science Letters 249, 47-61.

Griffin, W.L., Pearson, N.J., Belousova, E.A., Jackson, S.R., van Achterbergh, E., O'Reilly, S.Y., Shee, S.R. 2000. The Hf isotope composition of cratonic mantle: LAM-MC-ICPMS analysis of zircon megacrysts in kimberlites. Geochimica et Cosmochimica Acta 64, 133–147.

Griffin, W. L., Belousova, E. A., Walters, S. G., & O'Reilly, S. Y. 2006. Archaean and Proterozoic crustal evolution in the Eastern Succession of the Mt Isa district, Australia: U–Pb and Hf-isotope studies of detrital zircons*. Australian Journal of Earth Sciences 53, 125-149.

Griffin, W.L., Powell, W.J., Pearson, N.J. and O'Reilly, S.Y. 2008. GLITTER: data reduction software for laser ablation ICP-MS. In: Sylvester, P. Ed., Laser Ablation-ICP-MS in the Earth Sciences: Mineralogical Association of Canada Short Course Series 40, 204–207. Appendix 2.

Grimes, C.B., John, B.E., Kelemen, P.B., Mazdab, F.K., Wooden, J.L., Cheadle, M.J., Hanghoj, K., and Schwartz, J.J., 2007. Trace element chemistry of zir- cons from oceanic crust: A method for distinguishing detrital zircon prov- enance: Geology 35, 643–646.

Grimes, C. B., Wooden, J. L., Cheadle, M. J., & John, B. E. 2015. "Fingerprinting" tectono-magmatic provenance using trace elements in igneous zircon. Contributions to Mineralogy and Petrology 170, 1-26.

Hanchar, J. M., Finch, R. J., Hoskin, P. W., Watson, E. B., Cherniak, D. J., & Mariano, A. N. 2001. Rare earth elements in synthetic zircon: Part 1. Synthesis, and rare earth element and phosphorus doping. American Mineralogist 86, 667-680.

Harley, S. L. 1987. A pyroxene- bearing meta- ironstone and other pyroxene- granulites from Tonagh Island, Enderby Land, Antarctica: further evidence for very high temperature > 980° C Archaean regional metamorphism in the Napier Complex. Journal of Metamorphic Geology 5, 341-356.

Hofmann, A. E., Valley, J. W., Watson, E. B., Cavosie, A. J., & Eiler, J. M. 2009. Sub-micron scale distributions of trace elements in zircon. Contributions to Mineralogy and Petrology 158, 317-335

Hofmann, A. E., Baker, M. B., & Eiler, J. M. 2014. Sub-micron-scale trace element distributions in natural zircons of known provenance: implications for Ti-in-zircon thermometry. Contributions to Mineralogy and Petrology, 1683, 1-21.

Hoskin, P.W.O. 2005. Trace element composition of hydrothermal zircon and the alteration of Hadean zircon from the Jack Hills, Australia. Geochimica et Cosmochimica Acta, 69, 637–648.

Hoskin, P. W. O. and Schaltegger, U. 2003. The composition of zircon and igneous and metamorphic petrogenesis. In: Hanchar, J. M. & Hoskin, P.W.O. Eds Zircon. Reviews in Mineralogy and Geochemistry 53, 27–62

Jackson, S. E., Pearson, N. J., Griffin, W. L., & Belousova, E. A. 2004. The application of laser ablation-inductively coupled plasma-mass spectrometry to in situ U–Pb zircon geochronology. Chemical Geology 211, 47-69.

Kemp, A. I. S., Whitehouse, M. J., Hawkesworth, C. J., & Alarcon, M. K. 2005. A zircon U-Pb study of metaluminous I-type granites of the Lachlan Fold Belt, southeastern Australia: Implications for the high/low temperature classification and magma differentiation processes. Contributions to Mineralogy and Petrology 150, 230-249.

Košler, J., Sláma, J., Belousova, E., Corfu, F., Gehrels, G. E., Gerdes, A., ... & Whitehouse, M. J. 2013. U-Pb Detrital Zircon Analysis–Results of an Inter-laboratory Comparison. Geostandards and Geoanalytical Research 37, 243-259.

Kovaleva, E., Klötzli, U., Habler, G., & Wheeler, J. 2015. Planar microstructures in zircon from paleo-seismic zones. American Mineralogist 100, 1834-1847.

Kusiak, M. A., Whitehouse, M. J., Wilde, S. A., Nemchin, A. A., & Clark, C. 2013a. Mobilization of radiogenic Pb in zircon revealed by ion imaging: Implications for early Earth geochronology. Geology 41, 291-294.

Kusiak, M. A., Whitehouse, M. J., Wilde, S. A., Dunkley, D. J., Menneken, M., Nemchin, A. A., & Clark, C. 2013b. Changes in zircon chemistry during Archean UHT metamorphism in the Napier Complex, Antarctica. American Journal of Science 313, 933-967.

Luo, Y., & Ayers, J. C. 2009. Experimental measurements of zircon/melt trace element partition coefficients. Geochimica et Cosmochimica Acta 731, 3656-3679.

Matteini, M., Junges, S. L., Dantas, E. L., Pimentel, M. M., & Bühn, B. 2010. In situ zircon U–Pb and Lu–Hf isotope systematic on magmatic rocks: insights on the crustal evolution of the Neoproterozoic Goiás Magmatic Arc, Brasília belt, Central Brazil. Gondwana Research 17, 1-12.

Morel, M. L. A., Nebel, O., Nebel-Jacobsen, Y. J., Miller, J. S., & Vroon, P. Z. 2008. Hafnium isotope characterization of the GJ-1 zircon reference material by solution and laser-ablation MC-ICPMS. Chemical Geology 255, 231-235.

Nasdala, L., Hofmeister, W., Norberg, N., Martinson, J. M., Corfu, F., Dörr, W., ... & Frei, D. 2008. Zircon M257-a Homogeneous Natural Reference Material for the Ion Microprobe U-Pb Analysis of Zircon. Geostandards and Geoanalytical Research 32, 247-265.

Reddy, S.M., Timms, N.E., Trimby, P., Kinny, P.D., Buchan, C. and Blake, K, 2006 Crystal-plastic deformation of zircon: A defect in the assumption of chemical robustness. Geology 34, 257-260.

Reddy, S.M., Timms, N.E., Pantleon, W. and Trimby, P. 2007 Quantitative characterization of plastic deformation of zircon and geological implications. Contributions to Mineralogy and Petrology, 153, 625–645.

Reddy, S.M., Timms, N.E., Hamilton, .P.J. and Smyth, H.R. 2009 Deformation-related microstructures in magmatic zircon and implications for diffusion. Contributions to Mineralogy and Petrology 157, 231-244.

Reid, M. R., Vazquez, J. A., & Schmitt, A. K. 2011. Zircon-scale insights into the history of a Supervolcano, Bishop Tuff, Long Valley, California, with implications for the Ti-in-zircon geothermometer. Contributions to Mineralogy and Petrology 161, 293-311.

Rubatto, D. 2002. Zircon trace element geochemistry: partitioning with garnet and the link between U–Pb ages and metamorphism. Chemical Geology 184, 123-138.

Saxey, D. W., J. M. Cairney, D. McGrouther, T. Honma, and S. P. Ringer. 2007 Atom probe specimen fabrication methods using a dual FIB/SEM. Ultramicroscopy 107, 756-760.

Schaltegger, U., Fanning, C. M., Günther, D., Maurin, J. C., Schulmann, K., & Gebauer, D. 1999. Growth, annealing and recrystallization of zircon and preservation of monazite in high-

grade metamorphism: conventional and in-situ U-Pb isotope, cathodoluminescence and microchemical evidence. Contributions to Mineralogy and Petrology 134, 186-201.

Scherer, E. E., Whitehouse, M. J., & Münker, C. 2007. Zircon as a monitor of crustal growth. Elements 3, 19-24.

Schmitt, A. K., Wetzel, F., Cooper, K. M., Zou, H., & Wörner, G. 2010. Magmatic longevity of Laacher See Volcano Eifel, Germany indicated by U-Th dating of intrusive carbonatites. Journal of Petrology 51, 1053-1085.

Shannon, R. D. 1976. Revised effective ionic radii and systematic studies of interatomic distances in halides and chalcogenides. Acta Crystallography A32, 751-767.

Speer, J. A. 1980. Zircon. In P. H. Ribbe Ed., Orthosilicates. Review in Mineralogy Washington, DC, Mineralogical Society of America, pp. 67-112.

Spetsius, Z.V., Belousova, E.A., Griffin, W.L., O'Reilly, S.Y. and Pearson, N.J., 2002. Archean sulfide inclusions in Paleozoic zircon megacrysts from the Mir kimberlite, Yakutia: implications for the dating of diamonds. Earth and Planetary Science Letters 199, 111-126.

Timms, N., Kinny, P. and Reddy, S. 2006 Enhanced diffusion of Uranium and Thorium linked to crystal plasticity in zircon. Geochemical Transactions 7, 1-16.

Trimby, P. W. 2012. Orientation mapping of nanostructured materials using transmission Kikuchi diffraction in the scanning electron microscope. Ultramicroscopy 120, 16-24.

Trimby, P. W., Cao, Y., Chen, Z., Han, S., Hemker, K. J., Lian, J., ... & Wang, J. T. 2014. Characterizing deformed ultrafine-grained and nanocrystalline materials using transmission Kikuchi diffraction in a scanning electron microscope. Acta Materialia 62, 69-80.

Patchett, P. J., & Tatsumoto, M. 1981. A routine high-precision method for Lu-Hf isotope geochemistry and chronology. Contributions to Mineralogy and Petrology 75, 263-267.

Piazolo, S., Bestmann, M., Prior, D.J. and Spiers, C.J. 2006. Temperature dependent grain boundary migration in deformed-then-annealed material: Observations from experimentally deformed synthetic rocksalt. Tectonophysics 427, 55-71.

Piazolo, S., La Fontaine, A., Trimby, P., Harley, S., Yang, L., Armstrong, R., & Cairney, J. M. 2016. Deformation-induced trace element redistribution in zircon revealed using atom probe tomography. Nature communications, 7.

Prior, D.J., Wheeler, J., Peruzzo, L., Spiess, R. and Storey, C. 2002. Some garnet microstructures: an illustration of the potential of orientation maps and misorientation analysis in microstructural studies. Journal of Structural Geology 24, 999-1011.

Zheng, J., Griffin, W. L., O'Reilly, S. Y., Zhang, M., & Pearson, N. 2006. Zircons in mantle xenoliths record the Triassic Yangtze–North China continental collision. Earth and Planetary Science Letters 247, 130-142.

Valley, J.W., Cavosie, A.J., Ushikubo, T., Reinhard, D.A., Lawrence, D.F., Larson, D.J., Clifton, P.H., Kelly, T.F., Wilde, S.A., Moser, D.E. and Spicuzza, M.J., 2014. Hadean age for a post-magma-ocean zircon confirmed by atom-probe tomography. Nature Geoscience 7, 219-221.

Valley, J. W., Reinhard, D. A., Cavosie, A. J., Ushikubo, T., Lawrence, D. F., Larson, D. J., ... & Strickland, A. 2015. Presidential Address. Nano-and micro-geochronology in Hadean and Archean zircons by atom-probe tomography and SIMS: New tools for old minerals. American Mineralogist 100, 1355-1377.

Vavra, G. 1990. On the kinematics of zircon growth and its petrogenetic significance: a cathodoluminescence study. Contributions to Mineralogy and Petrology 106, 90-99.

Vervoort, J.D., Blichert-Toft, J., 1999. Evolution of the depleted mantle: Hf isotope evidence from juvenile rocks through time. Geochimica et Cosmochimica Acta 63, 533–556.

Wark, D. A., & Miller, C. F. 1993. Accessory mineral behavior during differentiation of a granite suite: monazite, xenotime and zircon in the Sweetwater Wash pluton, southeastern California, USA. Chemical Geology 110, 49-67.

Watson, E. B., & Cherniak, D. J. 1997. Oxygen diffusion in zircon. Earth and Planetary Science Letters 1483, 527-544.

Yuan, H. L., Gao, S., Dai, M. N., Zong, C. L., Günther, D., Fontaine, G. H., ... & Diwu, C. 2008. Simultaneous determinations of U–Pb age, Hf isotopes and trace element compositions

of zircon by excimer laser-ablation quadrupole and multiple-collector ICP-MS. Chemical Geology, 247, 100-118.

**Figure Captions**

**Figure 1** General characteristics of the gem quality, cm-sized GJ-1 standard (GJ-1/81); (a) optical image of the whole GJ standard grain confirming absence of cracks or any other structural disturbances; note there are also other grains of the GJ-1 standard shown; (b) CL image of GJ-1/81 segment revealing homogeneous signal throughout the grain; dark spots represent LA-ICPMS analysis pits.

**Figure 2** Results from quantitative orientation analysis (EBSD) of GJ-1/81 zircon; note the change in orientation is within analytical error; (a) EBSD map colour coded with relation to the change in crystallographic orientation of up to 2° relative to a reference orientation marked with a red cross; (b) profile across the grain marked as a black line in (a) showing change in orientation relative to orientation at the start of the profile (marked with a black spot).

**Figure 3** LA-ICPMS data showing the trace element composition and compositional homogeneity of GJ-1/81; for details on analysis procedure and data see text and Tables 1 and 2; the arrangement of trace elements is according to ionic radii following Shannon (1976); (a) example of chondrite normalised trace element pattern of GJ-1/81; (b) range of trace element data relative to average value derived from the 20 analysis spots shown as a grey field; inset shows the standard deviation and 1 sigma relative to the average; note the relatively large range in the light rare earth elements due to values being close to detection limit.

**Figure 4** Comparison of U/Yb and Y of GJ-1/81 and those of zircon from continental versus oceanic crustal zircons; LA-ICPMS data GJ-1/81 and fields as defined by Grimes et al. (2007).

**Figure 5** LA-ICPMS data showing the composition of the GJ-1/81 zircon relative to elemental composition of zircons from different origin (Belousova et al. 2002); (a) Y vs Yb/Sm, (b) Y vs Nb/Ta; c) Y vs U; d) Ce/Ce* vs. Eu/Eu* (Ce anomaly is given by Ce/Ce*, where Ce is the chondrite-normalised Ce concentration and Ce* is the average of the chondrite-normalised La and Pr concentrations. The Eu anomaly is calculated as Eu/Eu*, where Eu is the chondrite-normalised Eu value and Eu* is the average of the chondrite-normalised Sm and Gd concentrations).

**Figure 6** Comparison of Hf versus Y of GJ-1/81 and those of zircon from different origin; LA-ICPMS data GJ-1/81 and data from Belousova et al. (2002). Discrimination fields are defined by Hf/Y ratio and Zr/Hf ratio (shown in italic); the latter ratio can be shown in this diagram as Zr is a major constituent of zircon with near constant $ZrO_2$ concentrations of around 66wt% while Hf varies in a very broad range from around 0.5 to over 3wt% (e.g. Speer 1980, Belousova et al. 2002).

**Figure 7** Atomic scale characteristics of GJ-1/81 (a & b) and DN77 for comparison (c & d); DN77 stems from the Napier Complex, Antarctica (Harley 1987) and has been deformed crystal-plastically at high temperatures similar to zircons described in Piazolo et al. (2016). (a & c) three dimensional atomic scale chemical reconstruction derived from atom probe tomography; (b & d) orientation changes within atom probe tip illustrated by colour change from reference orientation marked with red cross; profile shows the change in orientation along the long axis of the tip; TKD analyses; for legend see (d); (a) atom probe tomography - chemical reconstruction of GJ-1/81; note chemical homogeneity within tip; (b) crystallographic orientation changes within atom probe tip GJ-1/81; note the lack of orientation change along the tip; stippled box shows section of ATP tip shown in (a); (c) atom probe tomography - chemical reconstruction of DN77; note the clustering of Y; (d) crystallographic orientation changes within atom probe tip DN77; note the systematic change in orientation across low angle boundaries; the location of these boundaries correlates with high Y areas shown in (c); stippled box shows section of ATP tip shown in (c).

**Table Captions**

**Table 1** Results from analysis on BCR-2 Columbia River Basalt reference material, which was analysed during this work versus U.S. Geological Survey Recommended/Information values.

**Table 2** LA-ICPMS trace-element data for the GJ-1/81 zircon; note error is provided as 1σ calculated using GLITTER (Griffin et al., 2008).

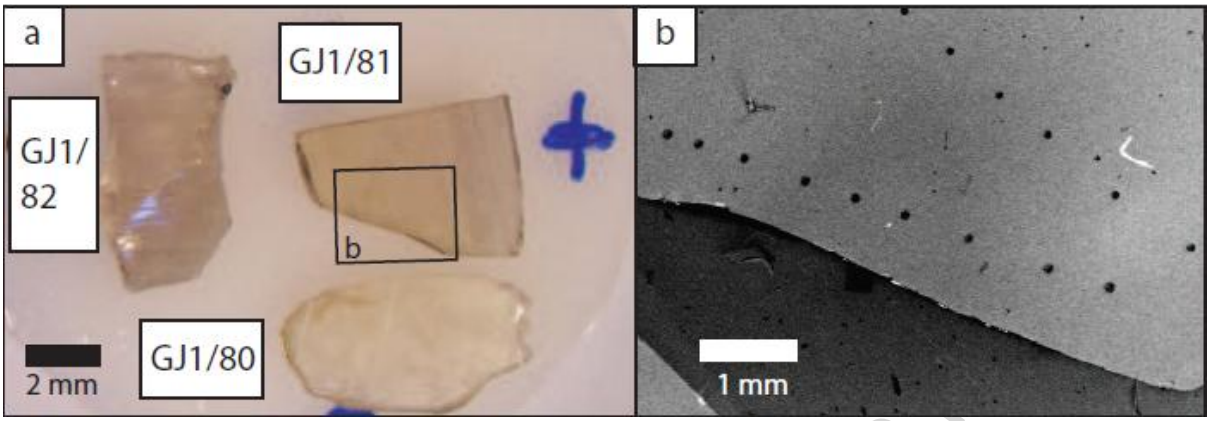


Figure 1

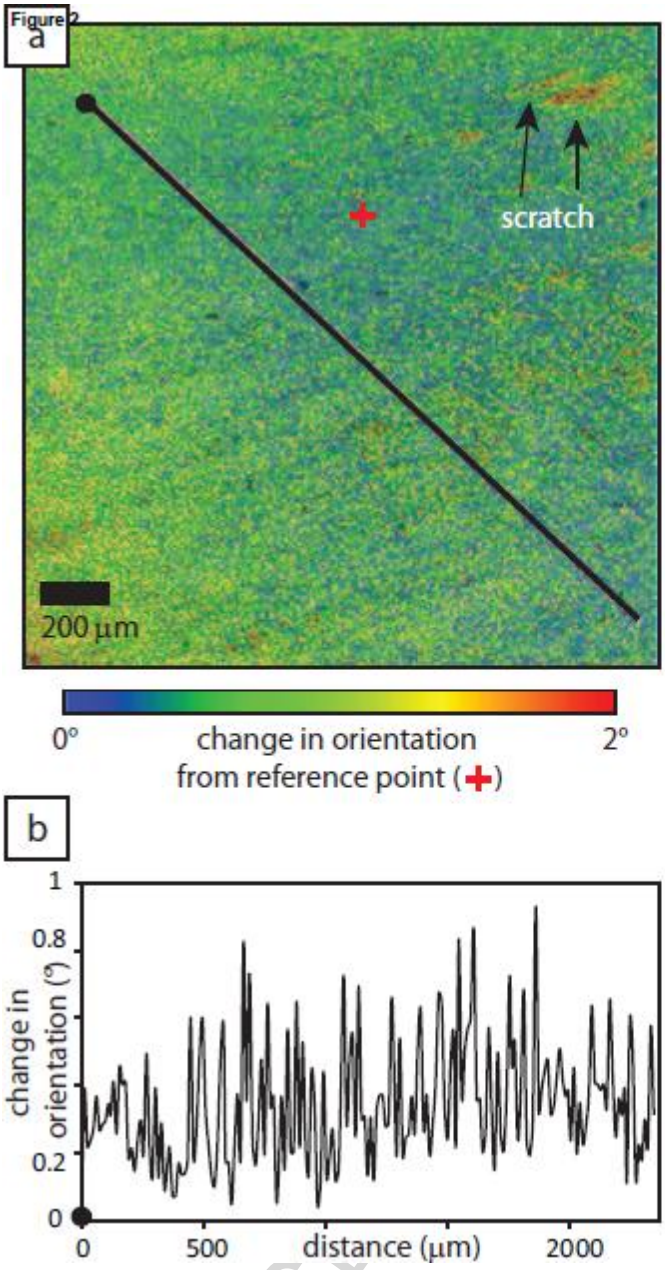


Figure 2

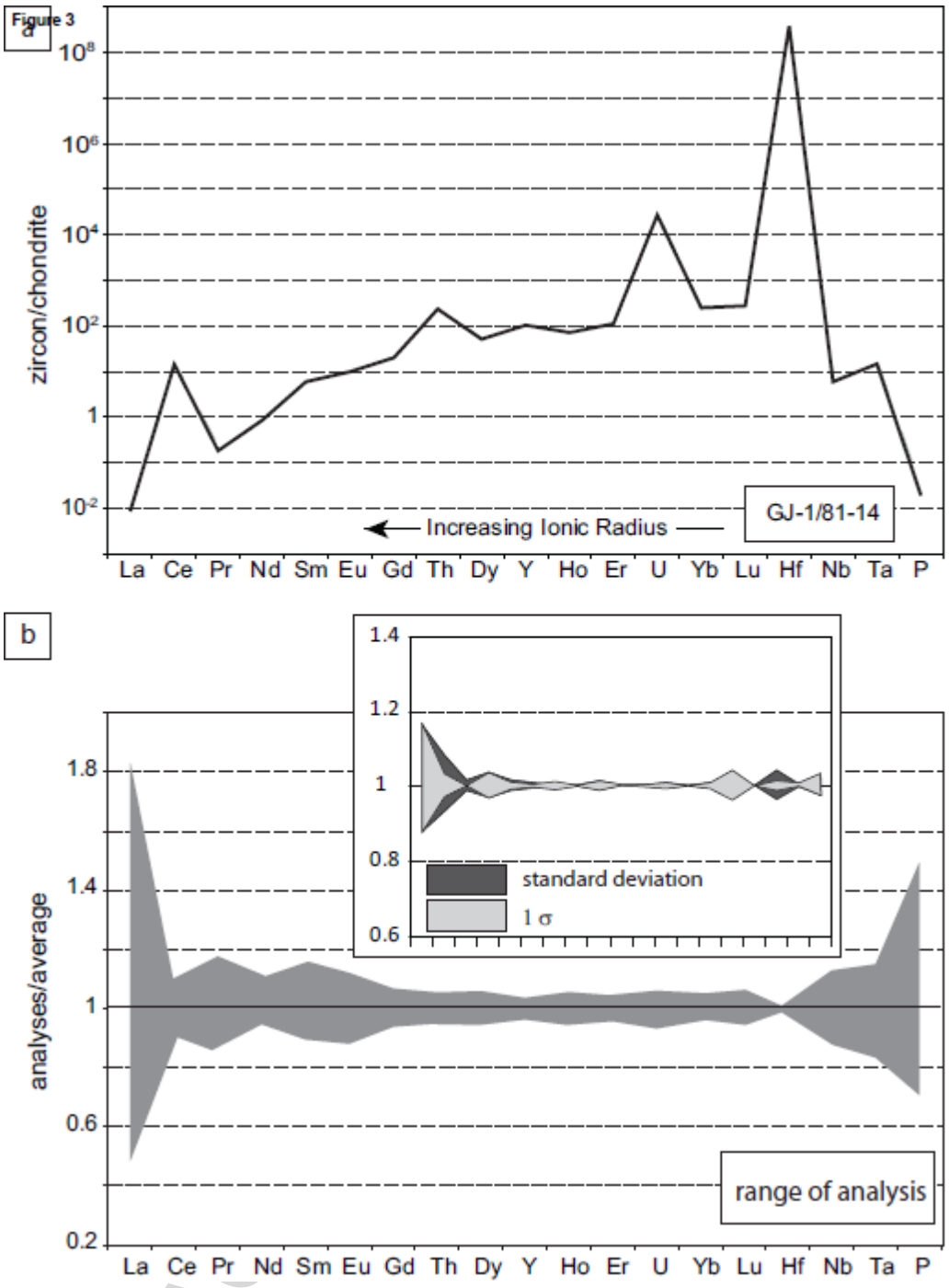


Figure 3

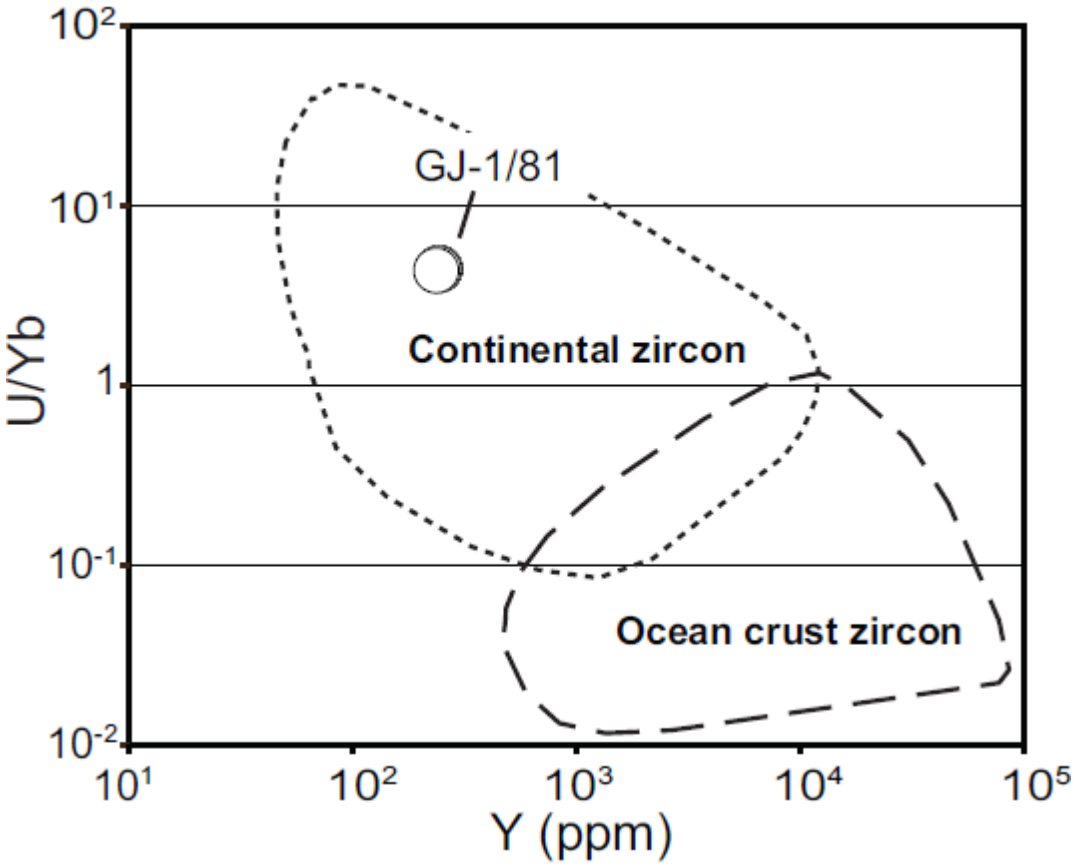


Figure 4

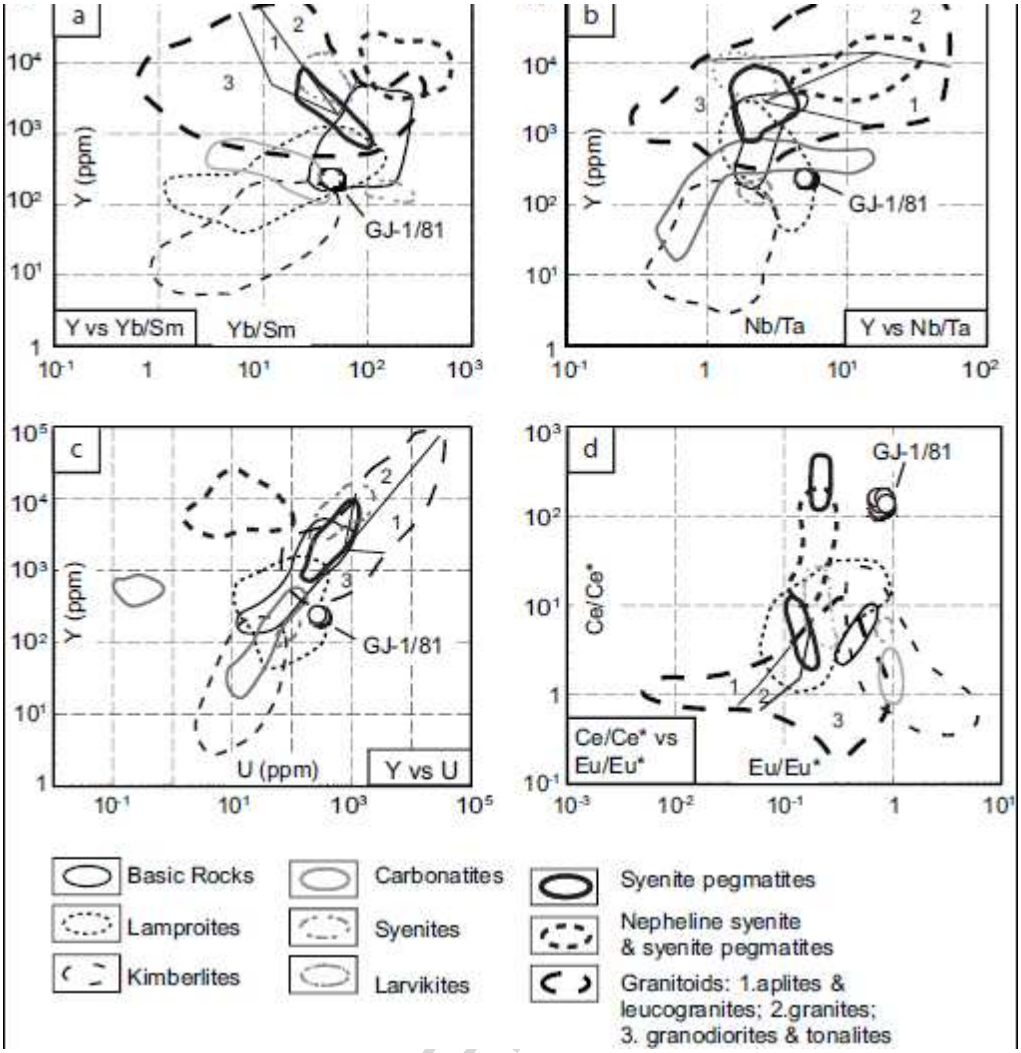


Figure 5

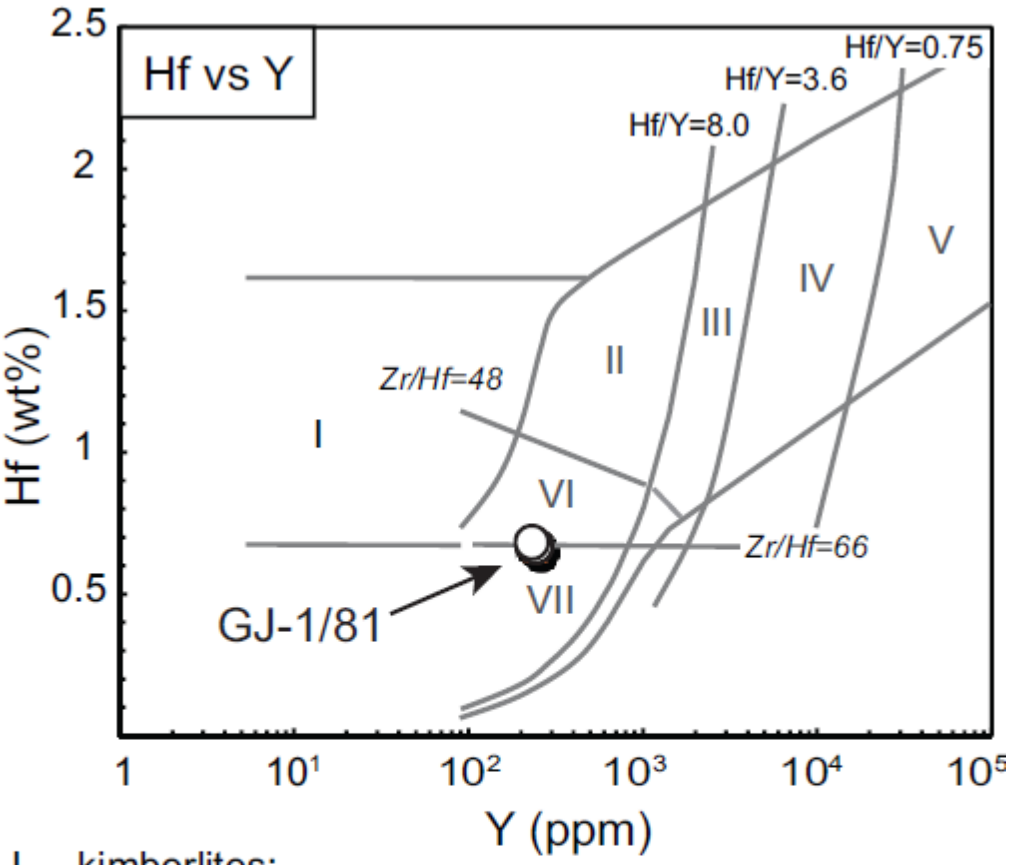


I -kimberlites;
II -ultrabasic, basic and intermediate rocks;
III -quartz-bearing intermediate and felsic rocks;
IV -felsic rocks with 'high' $SiO_2$ content;
V -greisens;
VI -alkaline rocks and alkaline metasomatites of alkaline complexes;
VII-carbonatites

Figure 6

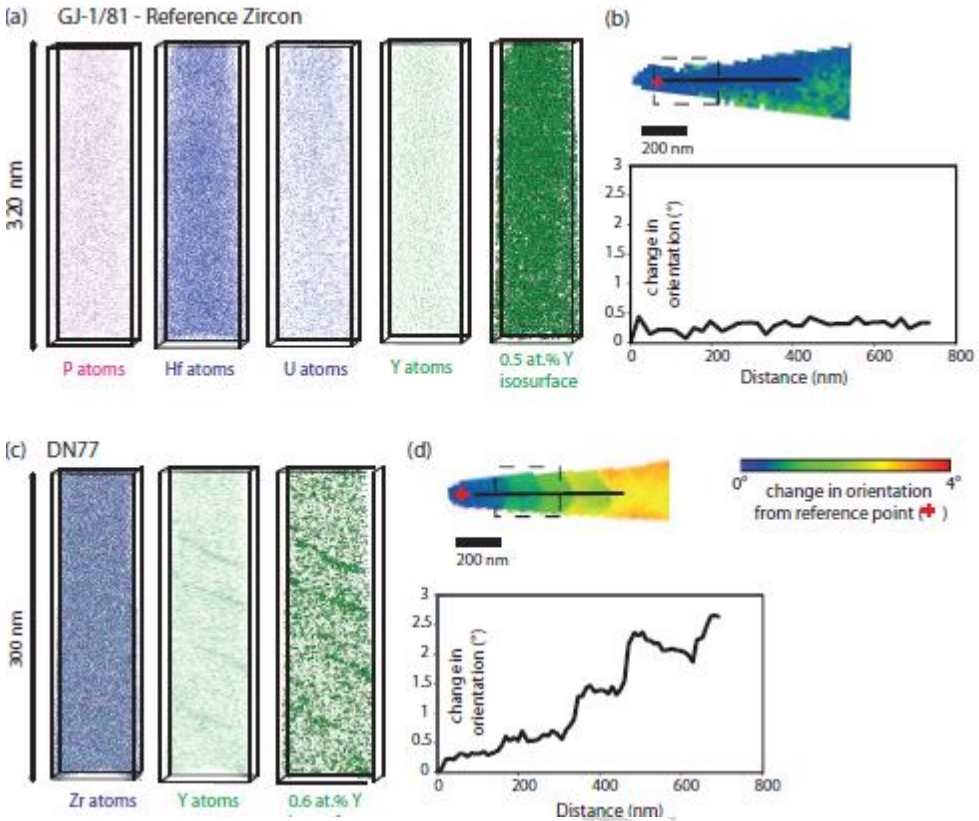


Figure 7

Table 1.

| Element | Mean (This study) ppm | 1sigma | USGS values* ppm | ± |
|---|---|---|---|---|
| Li | 9.88 | 0.50 | 9 | 2 |
| Mg | 21534 | 702 | 21600 | 300 |
| Al | 74448 | 2514 | 71400 | 1000 |
| P | 1266 | 204 | 1500 | 100 |
| Ti | 13694 | 453 | 13500 | 300 |
| V | 433 | 14 | 416 | 14 |
| Cr | 14.6 | 0.5 | 18 | 2 |
| Y | 32.05 | 3.25 | 37 | 2 |
| Mo | 238.79 | 7.53 | 248 | 17 |
| La | 24.80 | 0.79 | 25 | 1 |
| Ce | 51.78 | 1.61 | 53 | 2 |
| Pr | 6.50 | 0.21 | 6.8 | 0.3 |
| Nd | 28.80 | 0.94 | 28 | 2 |
| Sm | 6.43 | 0.25 | 6.7 | 0.3 |
| Eu | 1.98 | 0.07 | 2 | 0.1 |
| Gd | 6.03 | 0.23 | 6.8 | 0.3 |
| Tb | 0.98 | 0.04 | 1.07 | 0.04 |
| Ho | 1.23 | 0.04 | 1.33 | 0.06 |
| Tm | 0.48 | 0.02 | 0.54 | |
| Yb | 3.39 | 0.14 | 3.5 | 0.2 |
| Lu | 0.50 | 0.02 | 0.51 | 0.02 |
| Hf | 4.70 | 0.18 | 4.8 | 0.2 |
| Th | 5.88 | 0.19 | 6.2 | 0.7 |
| U | 1.79 | 0.06 | 1.69 | 0.19 |

*(https://crustal.usgs.gov/geochemical_reference_standards/basaltbcr2.html#information)

**Table 2. LA-ICPMS data (ppm) for the GJ-1/81 zircon standard**

| Analysis | Al | P | Ti | Cu | Ga | Ge | As | Rb | Y | Nb | Hf | Ta | Pb | Th | U |
|---|---|---|---|---|---|---|---|---|---|---|---|---|---|---|---|
| GJ1/81-01 | 3.83 | 45.2 | - | <0.05 | 0.10 | <0.16 | <0.19 | 0.09 | 243 | 1.80 | 6556 | 0.37 | 27.2 | 9.8 | 296 |
| GJ1/81-02 | 4.28 | 33.1 | - | 0.06 | 0.10 | 0.25 | <0.19 | 0.05 | 244 | 1.85 | 6635 | 0.37 | 27.2 | 9.9 | 300 |
| GJ1/81-03 | 4.2 | 33.1 | - | 0.06 | 0.11 | <0.16 | <0.21 | 0.05 | 244 | 1.81 | 6638 | 0.37 | 27.3 | 9.8 | 297 |
| GJ1/81-04 | 4.16 | 35.0 | - | 0.07 | 0.09 | <0.15 | 0.27 | 0.05 | 244 | 1.79 | 6668 | 0.34 | 27.4 | 10.1 | 296 |
| GJ1/81-05 | 4.23 | 38.6 | - | 0.06 | 0.10 | <0.16 | 0.22 | 0.06 | 244 | 1.79 | 6718 | 0.35 | 27.6 | 10.0 | 295 |
| GJ1/81-06 | 4.18 | 38.4 | - | 0.07 | 0.10 | 0.23 | <0.13 | 0.07 | 243 | 1.83 | 6673 | 0.35 | 27.3 | 10.0 | 297 |
| GJ1/81-07 | 4.35 | 31.0 | - | 0.07 | 0.11 | 0.17 | 0.20 | 0.10 | 245 | 1.83 | 6634 | 0.36 | 27.6 | 10.1 | 299 |
| GJ1/81-08 | 4.31 | 31.2 | - | 0.05 | 0.09 | <0.15 | 0.23 | 0.07 | 242 | 1.82 | 6631 | 0.36 | 27.2 | 10.0 | 293 |
| GJ1/81-09 | 3.98 | 33.4 | - | 0.05 | 0.09 | <0.15 | 0.21 | <0.04 | 243 | 1.80 | 6590 | 0.36 | 27.5 | 10.1 | 297 |
| GJ1/81-10 | 4.2 | 34.2 | - | 0.05 | 0.11 | <0.14 | <0.16 | 0.05 | 243 | 1.80 | 6622 | 0.36 | 27.2 | 10.2 | 296 |
| GJ1/81-11 | 3.42 | 33.1 | 3.26 | 0.06 | 0.23 | 0.14 | <0.10 | 0.07 | 235 | 2.25 | 6713 | 0.46 | 23.1 | 9.5 | 271 |
| GJ1/81-12 | 3.66 | 26.0 | 3.42 | 0.03 | 0.21 | <0.11 | 0.15 | 0.06 | 234 | 2.22 | 6762 | 0.44 | 23.4 | 9.5 | 273 |
| GJ1/81-13 | 3.75 | 23.7 | 3.18 | 0.07 | 0.20 | 0.16 | 0.22 | 0.07 | 233 | 2.24 | 6734 | 0.46 | 23.2 | 9.5 | 270 |
| GJ1/81-14 | 3.69 | 24.9 | 3.05 | 0.05 | 0.21 | 0.12 | 0.14 | 0.07 | 234 | 2.24 | 6734 | 0.44 | 23.2 | 9.4 | 271 |
| GJ1/81-15 | 3.72 | 25.3 | 3.19 | 0.10 | 0.21 | 0.11 | 0.11 | 0.08 | 234 | 2.26 | 6736 | 0.44 | 23.3 | 9.5 | 272 |
| GJ1/81-16 | 3.64 | 22.7 | 3.5 | 0.06 | 0.20 | 0.10 | 0.13 | 0.06 | 232 | 2.24 | 6704 | 0.45 | 23.0 | 9.4 | 268 |
| GJ1/81-17 | 3.66 | 24.7 | 3.46 | 0.07 | 0.21 | 0.10 | 0.13 | 0.07 | 232 | 2.20 | 6729 | 0.43 | 23.2 | 9.5 | 270 |

| | | | | | | | | | | | | | | |
|---|---|---|---|---|---|---|---|---|---|---|---|---|---|---|
| GJ1/81-18 | 3.67 | 23.9 | 3.29 | 0.08 | 0.20 | <0.10 | 0.13 | 0.06 | 233 | 2.19 | 6726 | 0.46 | 23.0 | 9.6 | 271 |
| GJ1/81-19 | 3.67 | 25.5 | 3.59 | 0.08 | 0.19 | <0.01 | <0.09 | 0.07 | 232 | 2.20 | 6683 | 0.44 | 23.1 | 9.5 | 268 |
| GJ1/81-20 | 3.68 | 21.8 | 3.57 | 0.07 | 0.21 | 0.19 | <0.11 | 0.06 | 232 | 2.14 | 6728 | 0.43 | 23.2 | 9.6 | 270 |
| Average | 3.91 | 30.2 | 3.35 | 0.06 | 0.15 | 0.16 | 0.18 | 0.07 | 238 | 2.01 | 6681 | 0.40 | 25.3 | 9.7 | 284 |
| 1SD | 0.29 | 6.4 | 0.18 | 0.01 | 0.06 | 0.05 | 0.05 | 0.01 | 5.4 | 0.21 | 57 | 0.05 | 2.1 | 0.3 | 14 |
| 1σ* | 0.15 | 6.2 | 0.18 | 0.02 | 0.01 | 0.05 | 0.06 | 0.01 | 7.6 | 0.07 | 218 | 0.02 | 3.19 | 0.33 | 9.5 |
| RSD (%) | 3.7 | 21 | 5.4 | 24 | 7.5 | 31 | 32 | 18 | 3.2 | 3.4 | 3.3 | 3.9 | 12.7 | 3.4 | 3.3 |

*1σ calculated using GLITTER 2008).

**Table 2 (cont.). LA-ICPMS data (ppm) for the GJ-1/81 zircon standard**

| Analysis | La | Ce | Pr | Nd | Sm | Eu | Gd | Tb | Dy | Ho | Er | Tm | Yb | Lu |
|---|---|---|---|---|---|---|---|---|---|---|---|---|---|---|
| GJ1/81-01 | 0.003 | 16.01 | 0.027 | 0.66 | 1.48 | 1.05 | 6.82 | 1.92 | 20.54 | 6.91 | 29.14 | 6.49 | 66.8 | 11.87 |
| GJ1/81-02 | <0.004 | 16.06 | 0.034 | 0.65 | 1.66 | 1.02 | 6.99 | 1.98 | 20.61 | 7.01 | 29.42 | 6.46 | 67.6 | 11.86 |
| GJ1/81-03 | 0.002 | 16.05 | 0.028 | 0.65 | 1.49 | 1.03 | 6.68 | 1.98 | 21.00 | 6.90 | 29.77 | 6.54 | 66.9 | 11.98 |
| GJ1/81-04 | 0.003 | 15.78 | 0.029 | 0.65 | 1.56 | 1.01 | 6.78 | 2.02 | 20.53 | 6.96 | 29.32 | 6.47 | 66.3 | 12.07 |
| GJ1/81-05 | <0.002 | 15.90 | 0.035 | 0.70 | 1.36 | 1.06 | 6.79 | 2.03 | 20.71 | 6.98 | 29.74 | 6.48 | 65.6 | 11.85 |
| GJ1/81-06 | <0.004 | 16.09 | 0.030 | 0.64 | 1.53 | 1.04 | 6.81 | 2.01 | 20.59 | 6.84 | 29.63 | 6.54 | 66.9 | 12.03 |
| GJ1/81-07 | 0.005 | 16.15 | 0.035 | 0.63 | 1.51 | 1.03 | 6.81 | 2.00 | 20.72 | 7.00 | 29.54 | 6.59 | 67.0 | 11.89 |
| GJ1/81-08 | <0.003 | 16.17 | 0.029 | 0.60 | 1.46 | 0.99 | 6.57 | 1.95 | 20.52 | 6.89 | 29.71 | 6.48 | 66.7 | 11.90 |
| GJ1/81- | <0.00 | 16.1 | 0.03 | 0.6 | 1.5 | 1.0 | 6.6 | 2.0 | 20.5 | 7.0 | 29.3 | 6.4 | 66. | 11.9 |

| | | | | | | | | | | | | | | |
|---|---|---|---|---|---|---|---|---|---|---|---|---|---|---|
| 09 | 4 | 1 | 0 | 6 | 0 | 3 | 6 | 0 | 9 | 2 | 7 | 8 | 0 | 6 |
| GJ1/81-10 | <0.003 | 16.02 | 0.034 | 0.62 | 1.52 | 1.04 | 6.72 | 1.99 | 20.42 | 6.94 | 29.58 | 6.41 | 66.4 | 12.07 |
| GJ1/81-11 | 0.003 | 13.87 | 0.030 | 0.61 | 1.42 | 0.88 | 6.45 | 1.75 | 19.43 | 6.47 | 27.79 | 6.28 | 62.2 | 11.08 |
| GJ1/81-12 | <0.002 | 13.82 | 0.027 | 0.63 | 1.37 | 0.85 | 6.43 | 1.80 | 19.62 | 6.49 | 28.22 | 6.27 | 63.4 | 11.11 |
| GJ1/81-13 | 0.002 | 13.77 | 0.027 | 0.63 | 1.41 | 0.89 | 6.56 | 1.78 | 19.39 | 6.44 | 27.78 | 6.27 | 62.7 | 11.11 |
| GJ1/81-14 | <0.002 | 13.79 | 0.026 | 0.60 | 1.37 | 0.90 | 6.26 | 1.78 | 19.48 | 6.47 | 27.93 | 6.36 | 62.8 | 11.07 |
| GJ1/81-15 | 0.001 | 13.85 | 0.026 | 0.61 | 1.39 | 0.86 | 6.61 | 1.79 | 19.22 | 6.58 | 28.05 | 6.34 | 63.3 | 11.13 |
| GJ1/81-16 | 0.001 | 13.70 | 0.031 | 0.63 | 1.29 | 0.88 | 6.41 | 1.76 | 19.23 | 6.48 | 27.82 | 6.34 | 62.9 | 11.03 |
| GJ1/81-17 | 0.002 | 13.59 | 0.033 | 0.63 | 1.45 | 0.88 | 6.59 | 1.80 | 19.43 | 6.42 | 28.08 | 6.33 | 62.7 | 11.14 |
| GJ1/81-18 | 0.003 | 13.83 | 0.029 | 0.60 | 1.38 | 0.90 | 6.27 | 1.77 | 19.49 | 6.47 | 28.03 | 6.31 | 63.1 | 11.14 |
| GJ1/81-19 | 0.003 | 13.79 | 0.029 | 0.63 | 1.34 | 0.90 | 6.37 | 1.77 | 19.20 | 6.47 | 27.87 | 6.25 | 63.2 | 11.03 |
| GJ1/81-20 | <0.002 | 13.74 | 0.026 | 0.60 | 1.40 | 0.88 | 6.53 | 1.80 | 19.41 | 6.44 | 27.72 | 6.33 | 63.2 | 11.02 |
| Average | 0.003 | 14.9 | 0.030 | 0.63 | 1.44 | 0.96 | 6.66 | 1.88 | 20.0 | 6.7 | 28.7 | 6.4 | 64.8 | 11.52 |
| 1SD | 0.001 | 1.16 | 0.003 | 0.03 | 0.09 | 0.08 | 0.20 | 0.11 | 0.65 | 0.25 | 0.84 | 0.10 | 1.9 | 0.45 |
| 1σ* | 0.001 | 0.48 | 0.00 | 0.03 | 0.06 | 0.04 | 0.24 | 0.06 | 0.66 | 0.22 | 0.92 | 0.21 | 2.09 | 0.37 |
| RSD (%) | 41 | 3.2 | 8.9 | 5.4 | 4.4 | 3.8 | 3.6 | 3.4 | 3.3 | 3.3 | 3.2 | 3.3 | 3.2 | 3.2 |

*1σ calculated using GLITTER 2008).

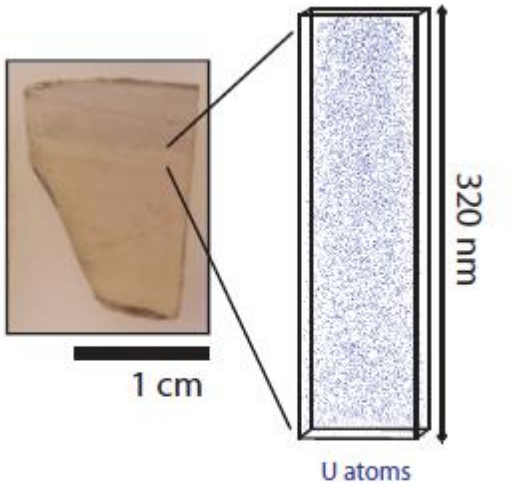


Graphical abstract